Solution multistability in first-order nonlinear differential delay equations

Jérôme Losson
Department of Physics and Center for Nonlinear Dynamics, McGill University, 3655 Drummond, Montréal, Québec, H3G-1Y6, Canada

Michael C. Mackey
Departments of Physiology, Physics, and Mathematics, and Center for Nonlinear Dynamics, McGill University, 3655 Drummond, Montréal, Québec, H3G-1Y6, Canada

André Longtin
Département de Physique, Université d'Ottawa, 150 Louis Pasteur, Ontario, K1N-6N5, Canada

(Received 19 June 1992; accepted for publication 29 January 1993)

The dependence of solution behavior to perturbations of the initial function (IF) in a class of nonlinear differential delay equations (DDEs) is investigated. The structure of basins of attraction of multistable limit cycles is investigated. These basins can possess complex structure at all scales measurable numerically although this is not necessarily the case. Sensitive dependence of the asymptotic solution to perturbations in the initial function is also observed experimentally using a task specific electronic analog computer designed to investigate the dynamics of an integrable first-order DDE.

I. INTRODUCTION

The set formed by all the points in the phase space of a dynamical system which are attracted to a given solution (e.g., a fixed point, a limit cycle, or a chaotic solution) is called the basin of attraction of that solution. Some analytic maps and many nonlinear dynamical systems possess coexisting solutions (referred to as multistable solutions), and different initial conditions, belonging to different basins of attraction will be attracted to the corresponding solutions. The boundaries of the various basins of attraction are known as basin boundaries.

Sensitive dependence of a dynamical system's temporal evolution to perturbations of the initial conditions is ubiquitous in nonlinear dynamics. Many investigations, dating back to the pioneering work by Julia and Fatou[1,2] at the end of the 19th century, have focused on the geometry of basin boundaries of multistable analytic maps of the complex plane. It is now clear that some of these transformations possess what are known as fractal basin boundaries. Recently, a number of investigators, including Grebogi, McDonald, Ott and Yorke (see Refs. 3–5 and references therein), have discussed the geometry of basin boundaries in nonlinear return maps obtained from ordinary differential equations (ODEs) and demonstrated the fractal nature of these boundaries in various one- and two-dimensional cases. This paper focuses on the dependence of solution behavior on the initial conditions in certain first-order nonlinear DDEs.

DDEs have been the focus of intense study in the past decade because their solutions may exhibit chaos, and, in particular, high-dimensional chaos.[6,7] They have been used to describe the dynamics of laser systems,[8–12] physiological control systems,[13–15] and artificial neural network models,[16] and to explain the oscillations observed in agricultural commodity prices.[17] DDEs have also received considerable attention in the applied mathematics literature because, through a singular perturbation limit procedure, they are a natural continuous time extension of discrete-time maps.[18,19] Electro-optic[20] and acousto-optic[21] devices have been successfully designed to study the dynamics of DDEs. Vallée and Delisle[22] showed experimentally how the most unstable mode of the linearized DDE enslaves all the other modes, and how blocking it leads to the appearance of another period-doubling sequence starting with the second mode. There have been a small number of numerical studies of hysteresis due to the coexistence of periodic and chaotic solutions of DDEs.[23,9,21] Ikeda *et al.*[23] have argued that the number of coexisting harmonic solutions of the laser equation studied in Ref. 11 was less than, but proportional to, the delay.

Work on these hybrid analog computers and the corresponding numerical investigations have focused mainly on the analysis of routes to chaos, but the stability of limit cycles with respect to changes in the initial functions has, to now, received little attention. Two notable exceptions are the works of Aguirregabiria and Etxebarria[24] and Li and Hao.[25] The former have investigated the structure of basin boundaries for a delayed Duffing equation. They studied the system with a class of periodic initial functions parametrized by the frequency, and demonstrated the existence of self-similar structure in a subset of the boundary separating nonchaotic attractors. However, the system they considered displayed multistability even without the delay. A preliminary study of the basins of attraction of two periodic solutions of a first-order DDE was undertaken by Li and Hao[25] who were investigating bistability in an equation introduced by Zhang *et al.*[12] to describe a liquid crystal hybrid optical bistable device. They did not report on the structure of the boundary at various scales, and our results of Sec. III indicate that there is a nontrivial dependence of solution behavior on perturbations of the initial functions (IFs), whatever the scale of this perturbation, in systems similar to those considered by these authors.

Except for the single report by Li and Hao, there are

 1054-1500/93/020167-10$06.00

no results concerning the structure of basin boundaries for equations that do not display multistability when the delay term is eliminated. Here, we demonstrate the presence of multistability in DDEs and show that the structure of the basin boundaries can be complex at all (numerically) measurable scales. Preliminary analog studies of a first-order integrable DDE also suggest that multistability is ubiquitous for nonmonotone nonlinearities, and that the structure of the basin boundaries separating multistable limit cycles possesses a complicated geometry on scales ranging over several orders of magnitude. Though it is impossible to rigorously demonstrate self-similar properties with an analog computer, using such a device allows one to comment on the robustness of the basin geometry under the influence of the stochastic perturbations present due to the inherent noise in analog devices.

The paper is organized as follows. In Sec. II, we introduce the class of nonlinear DDEs on which we focus. Bistability is discussed in two first-order DDEs with smooth nonlinearities: the logistic DDE and the Mackey–Glass equation. The bistability is explored with sinusoidal IFs parametrized by their frequency. Section III considers a nonlinear integrable DDE introduced by an der Heiden and Mackey[26] as a paradigm for mixed delayed feedback loops. Higher-order multistability is discussed, and the basin boundaries are explored with a class of nonconstant IFs. It is shown numerically that the boundaries can possess intricate structure at all scales. A task specific electronic analog computer, designed to integrate the DDE of Sec. III, is described in Sec. IV. Hysteresis and multistability are present in the analog computer and confirm the robustness of the results of Sec. III.

II. FIRST-ORDER NONLINEAR DDEs

We consider the dynamics of nonlinear first-order differential delay equations. The equations describe the evolution of a variable x which is being destroyed at a rate α, and produced, with some delay, via a nonlinear production mechanism:

$$\frac{dx}{dt}=-\alpha x+F(x_\tau) \quad \text{for} \quad t\geqslant 0, \quad x_\tau\equiv x(t-\tau), \tag{1}$$

where τ, $\alpha>0$, and F (the *feedback function*) is the rate of production which depends on the history of the variable. Throughout this paper, the initial function for Eq. (1) is denoted by $\varphi(t)$:

$$x(t)\equiv\varphi(t) \quad \text{for } t\in[-\tau,0).$$

The wealth of dynamics displayed by Eq. (1) depends to a great extent on the characteristic of the feedback F.[26] We are interested here in the case where F is nonmonotone, modeling so-called *mixed feedback* control loops. In this case the rate of production is maximal for some intermediate value of the delayed variable. Although Eq. (1) looks simple, it corresponds to a class of semidynamical systems which can display a remarkable range of solutions: steady states bifurcating to limit cycles of arbitrary complexity to chaotic trajectories as a control parameter is varied. The dimension of the chaotic attractors for the solutions of (1) was studied by Farmer[7] who found that it was an increasing function of the delay.

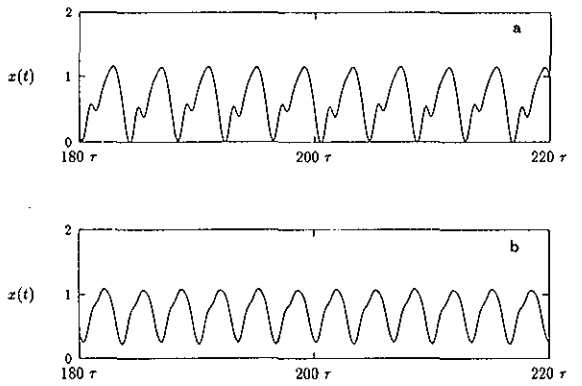

FIG. 1. Two coexisting solutions of (2). The parameter values in both cases are $\alpha=1$, $\lambda=5.81$, $\tau=1$. (a) The initial function is $\varphi(t)=0.4\sin(0.3t)+0.5$. (b) The initial function is now $\varphi(t)=0.4\sin(1.3t)+0.5$.

In the next section, we illustrate solution dependence on perturbations of the initial function in three such DDEs.

A. The "logistic" DDE

The so-called logistic DDE is Eq. (1) with a quadratic feedback function F:

$$\frac{dx}{dt}=-\alpha x+\lambda x_\tau(1-x_\tau), \quad \lambda,\alpha\in\mathbb{R}. \tag{2}$$

This DDE takes its name from the observation that it is obtained by performing a *singular perturbation limit* procedure on the celebrated logistic map

$$x_{n+1}=\tilde{\lambda}x_n(1-x_n), \quad \text{where} \quad \tilde{\lambda}\equiv\lim_{\lambda,\alpha\to\infty}\frac{\lambda}{\alpha}. \tag{3}$$

The DDE (2) therefore provides us with a continuous time extension of the logistic map (3). This link between maps and DDEs has been used in the literature to extend some results concerning the dynamics of the former to the more challenging continuous time situation. For a review of such results, see Ivanov and Sharkovskiĭ.[19]

Figure 1 displays two coexisting solutions of Eq. (1) which are obtained with sinusoidal initial functions

$$\varphi(t)=A\sin(\omega t)+B, \quad A,\omega\in\mathbb{R}_1^+ \quad B\in\mathbb{R}.$$

The only difference between the situation giving rise to the solutions in Figs. 1(a) and 1(b) is the frequency ω of the sinusoidal initial function $\varphi(t)$. The algorithm used for the integration of this equation (and the Mackey–Glass equation, Sec. II B) is based on an adaptive step size sixth-order Verner method. The delayed term is located and the solution at this point is interpolated with a three-point Hermite interpolation scheme. (Because of memory constraints, the basins of attraction were investigated using a simpler version of this code using a fourth-order Runge–Kutta and a linear interpolation scheme. The stability of the simpler

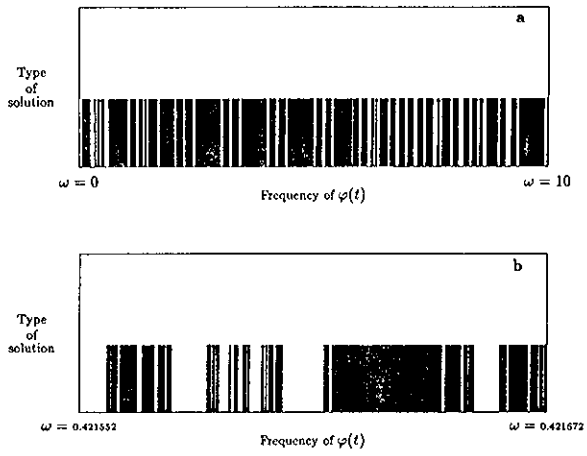

FIG. 2. This figure displays which values of ω [the frequency of the initial function $\varphi(t)$ of Eq. (2)] give rise to the solution of Fig. 1(b), keeping all other parameters at the values specified in Fig. 1. The vertical bars are placed at the values of ω giving rise to the solution displayed in Fig. 1(b). When a vertical bar is not present for a given ω, the corresponding solution of Eq. (2) is the one displayed in Fig. 1(a). In part (a), the DDE (2) was solved with 5000 different values of ω uniformly distributed between 0 and 10. In part (b), (2) was solved with 5000 different values of ω uniformly distributed between 0.421 552 and 0.421 672. No other types of oscillatory solutions were observed for these parameter values. The time t_c of convergence to the asymptotic limit cycle ranges from $t_c \sim 10$ delays to $t_c \sim 6000$ delays, depending on ω in a complex manner.

version of the algorithm was checked thoroughly and the latter could hence be used as a reasonable and efficient substitute for the original code.)

The presence of bistability in this system is not very surprising since it has been reported previously by Li *et al.* in a similar DDE arising from modeling the dynamics of nonlinear optical cavities.[25,12] The surprising aspect of this bistability is shown in Fig. 2 where we plot the occurrence of the solution in Fig. 1(b) as a function of the frequency of the initial function. Figure 2 is therefore a glimpse at the structure of the basins of attractions of different limit cycle

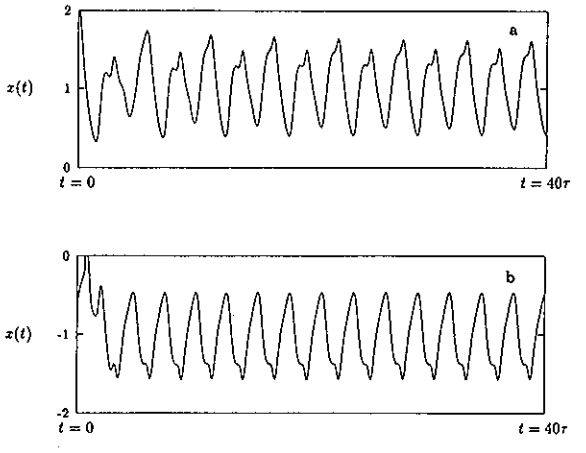

FIG. 3. Two bistable solutions of the Mackey–Glass equation. The parameters in both panels are $\alpha=1$, $\beta=3$, $n=8$, $\tau=1.25$. The initial function in both is $\varphi(t)=1.5\sin(\omega t)+0.6$. (a) $\omega=0.3$; (b) $\omega=0.7$. The transients are specific to the initial functions, and Fig. 4 displays the limiting asymptotic solutions evolving from (a) and (b) shown here.

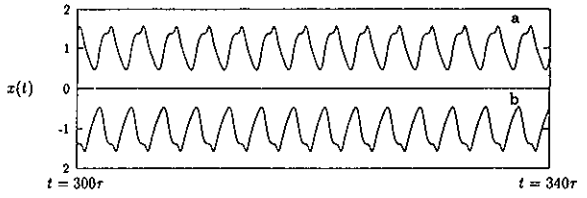

FIG. 4. The positive and negative bistable solutions of the Mackey–Glass equation after sufficiently long transients. The parameters are those of Fig. 3.

solutions of (2). Our digital solutions indicate that this structure is clearly intricate at all possible scales of numerical investigation.

B. The Mackey–Glass equation

The Mackey–Glass equation,[27]

$$\frac{dx}{dt} = -\alpha x + \frac{\beta x_\tau}{1+x_\tau^n}, \tag{4}$$

was introduced in an attempt to explain the oscillations in numbers of neutrophils observed in some cases of chronic myelogenous leukemia. The most striking feature of this equation is that when the exponent n in the feedback function is even, or when the feedback function becomes $F=\beta x_\tau/(1+|x_\tau|^n)$, the equation is invariant under the transformation $x(t)\rightarrow -x(t)$. As a consequence, if $x(t)$ is a limit cycle solution of (4), $-x(t)$ is also a solution. This bistability is illustrated in Fig. 3 (and Fig. 4).

Although it is easy to understand the origin of this behavior, the stability of the various limit cycles remains to be classified. This classification amounts to studying the structure of the basins of attractions. From a modeling perspective, it is important to know whether one might expect to observe both kinds of solutions experimentally (given a small uncertainty in the initial preparation) or whether the initial functions giving rise to different solutions differ in a "radical" way.

In Fig. 5 we plot the values of the frequency ω which eventually yield strictly positive or negative solutions. The structure of the basin of attraction in this case is obviously much simpler than for the quadratic nonlinearity, but again this is a consequence of symmetry in the Mackey–

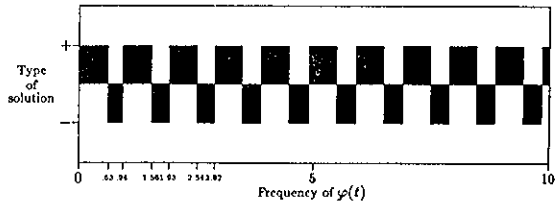

FIG. 5. This figure displays the values of ω giving rise to positive and negative limit cycles of Eq. (4). The vertical bars above 0 indicate that at that value, the asymptotic solution is the positive limit cycle displayed in Fig. 3(a). The vertical bars going from 0 to -1 indicate that at that value of ω the asymptotic limit cycle is the negative solution shown in Fig. 3(b).

Glass equation. Note, however, that relatively small perturbations to the initial functions can alter the evolution of the system in a dramatic way.

Obtaining figures like 2 and 5 is computationally expensive. It is therefore desirable to focus on a nonlinear DDE which is analytically tractable (and hence computationally more efficient), but which is known to display the spectrum of dynamics characteristic of first-order nonlinear DDEs. The dynamics of such a system can then be linked analytically to the behavior of realistic models. In the next section we investigate such an equation, introduced by an der Heiden and Mackey[26] as a paradigm for delayed mixed feedback mechanisms.

III. THE PIECEWISE CONSTANT MODEL

an der Heiden and Mackey[26] have studied Eq. (1) with a piecewise constant nonlinearity:

$$\frac{dx}{dt}=-\alpha x+F(x_\tau), \tag{5a}$$

where

$$F(s)=\begin{cases} c & \text{if } s\in[\theta_1,\theta_2], \\ 0 & \text{if } s<\theta_1 \text{ or } s>\theta_2, \end{cases} \tag{5b}$$

and c, $\theta_2>\theta_1$ are also positive constants. One can think of the piecewise constant forcing as the simplest idealization of more realistic smooth nonmonotone functions. An immediate consequence of this choice for F is that (1) can now be integrated analytically:

$$x(t)=\begin{cases} x(t_0)e^{-\alpha(t-t_0)}, & \text{if } x_\tau<\theta_1 \text{ or } x_\tau>\theta_2, \\ \gamma+(x(t_0)-\gamma)e^{-\alpha(t-t_0)}, & \text{if } x_\tau\in[\theta_1,\theta_2], \end{cases} \tag{6}$$

where $\gamma\equiv c/\alpha$ is the asymptote of the increasing exponential segment. Thus the solution of (5) is a sequence of either increasing or decreasing exponential segments depending on the value of the variable x a time τ ago.

Despite its simplicity, Eq. (5) can exhibit solutions ranging from simple fixed points to wildly oscillating chaotic trajectories.[26] Since (5) is analytically integrable, one may use a digital computer to keep track of the crossing times of the solution with the thresholds θ_1 and θ_2. (Details of an analytic integration algorithm for (5) can be found in Ref. 28. The algorithm used to produce the figures of this section is given in Ref. 29.) The solution is determined uniquely by these crossing times, rather than by all values of $x(t)$ within one delay interval. In fact, for fixed $x(0)$, the solution depends solely on the crossing times within the initial function.[26] This "reduction in dimensionality" enabled an der Heiden and Mackey[26] to analytically prove [for Eq. (5)] the existence of limit cycles, of a homoclinic orbit, and of Li and Yorke-type chaos, and to characterize the global stability of simple limit cycles (i.e., with one maximum per period), also known as "slowly oscillating periodic solutions." Further, an der Heiden[18] was able to prove that the map governing the crossing times was *exact* (cf. Ref. 30) for certain parameters, implying that the crossings occur very irregularly. These results have been shown to also hold when the discontinuities

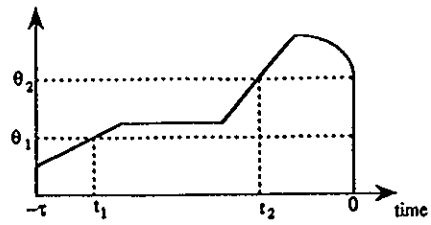

FIG. 6. Graph of an initial function $\varphi\in\mathscr{I}$.

of F are smoothed out,[31,32] making the results more relevant to real physical systems. This observation, combined with the existence of analytical results concerning its global stability, motivated our choice to simulate Eq. (5).

The fact that a trajectory is uniquely determined by $x(-\tau)$, $x(0)$ and the times at which the initial function crosses θ_1 or θ_2 on the interval $[-\tau,0]$ is important because it allows us to parametrize a class $\mathscr{I}$ of nonconstant initial functions in a natural way: Let φ defined on $[-\tau,0]$ be an initial function for Eq. (5) and pick t_1, t_2 such that $-\tau\leqslant t_1<t_2\leqslant 0$. If

$$\varphi(t)<\theta_1 \quad \text{for} \quad t\in[-\tau,t_1), \quad \varphi(t_1)=\theta_1,$$

$$\varphi(t)\in(\theta_1,\theta_2) \quad \text{for} \quad t\in(t_1,t_2), \quad \varphi(t_2)=\theta_2,$$

$$\varphi(t)>\theta_2 \quad \text{for} \quad t\in(t_2,0), \quad \varphi(0)=\theta_2$$

then $\varphi\in\mathscr{I}$ (see Fig. 6).

A. Higher-order multistability

In this section we explore the sensitivity of limit cycle solutions of Eq. (5) to variations in some nonconstant initial conditions. We restrict our attention to initial functions $\varphi\in\mathscr{I}$.

Figure 7 displays bistable limit cycles of (5) obtained with two different initial functions φ_1 and φ_2 in $\mathscr{I}$ with α, θ_1, θ_2, c, and τ held constant. Figure 8 displays tristable solutions of Eq. (5). This type of multistability in DDEs has not been previously reported. Note that this behavior is

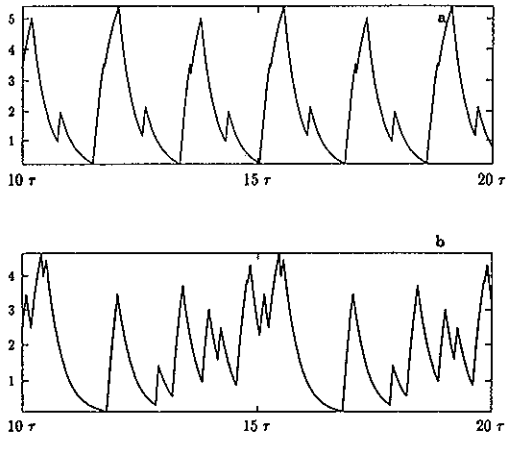

FIG. 7. Typical co-existing solutions of Eq. (5) and initial functions $\varphi\in\mathscr{I}$. The parameters are: $\alpha=3.25$; $c=20.5$; $\tau=1$; $\theta_1=1$; $\theta_2=2$. For (a) $t_1=-0.9925$; $t_2=-0.6$; and the period is $P=3.66$. In (b) $t_1=-0.995$; $t_2=-0.27$; and the period is $P=5.19$.

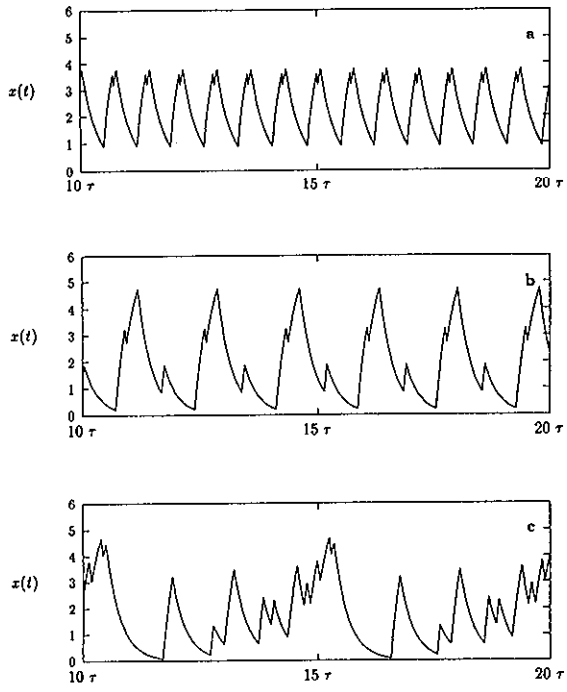

FIG. 8. Illustration of multistability in Eq. (5). The parameters are the same as in Fig. 7, except $\alpha=3.75$. For (a) $t_1=-0.925$; $t_2=-0.711$; and the period is $P=0.75$. (b) $t_1=-0.9$; $t_2=-0.386$; and $P=1.78$. (c) $t_1=-0.9925$; $t_2=-0.4$; and $P=5.05$.

robust in the sense that it is observed for large regions of parameter space. This is illustrated in Fig. 9 where we plot of the periods of the solutions of (5) obtained with a variety of initial functions $\varphi\in\mathscr{I}$ as the parameter c is varied with α, θ_1, θ_2, τ held constant. Figure 9 illustrates the relative predominance of short limit cycles (containing at most four extrema per period), an example of which is displayed in Fig. 8(a). Long limit cycles are less common than their short period counterparts. (Although it appears in Fig. 9 that there is no change in the period of the short limit cycles as c increases, there is in fact a slight decrease of the period, but it is unobservable because of the logarithmic plotting of the ordinate.)

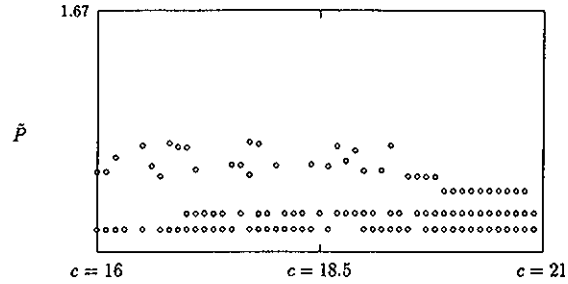

FIG. 9. The quantity $\tilde{P}\equiv\log(1+\log(1+P))$ as the parameter c is varied for $\tau=1$, $\alpha=3.25$, $\theta_1=1$, and $\theta_2=2$. $\tilde{P}$ was plotted here rather than P, the period of limit cycle solutions of (5), for the clarity of the figure.

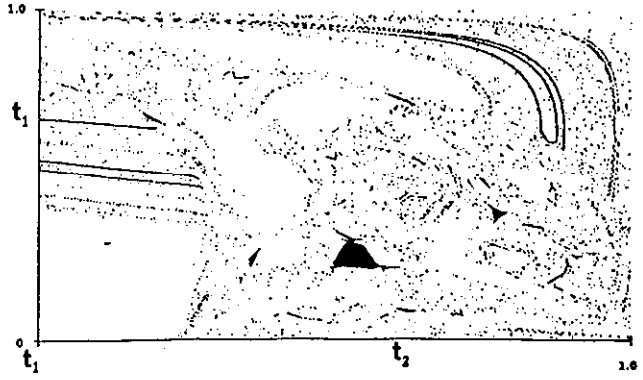

FIG. 10. Subsets of the basins of attraction of two bistable solutions of (5) displayed in Figs. 7(a) and 7(b). The black dots represent values of (t_1,t_2) such that $\varphi\in\mathscr{I}$ generates the solution of Fig. 7(a). More precisely, for each t_1, the graphs represents 1000 values for t_2 distributed uniformly between t_1 and 0, and the procedure is repeated for 1000 values of t_1. The plotted points represent the loci in (t_1,t_2) space which generate the short limit cycle solution of Fig. 7(a). [Areas void of plotted points correspond to values of (t_1,t_2) which generate other types of solutions of Eq. (5): i.e., the long period limit cycle solutions of Fig. 7(b) or asymptotically nonoscillatory solution tending to γ or 0.]

B. Basins of attraction

Given a fixed set of parameters $(\alpha, \theta_1, \theta_2, \tau, c)$ for Eq. (5), what is the relative distribution of long and short limit cycles in (t_1,t_2) space? This question is more crucial than the simple determination of the presence of multistable behavior, since it quantitatively addresses the sensitivity of the solutions to variations of the parameters t_1 and t_2.

Consider Eq. (5) with the parameters used to generate Fig. 7. As t_1 and t_2 are varied, we expect to generate both types of solutions presented in Figs. 7(a) and 7(b). Figure 10 represents the solution types of Eq. (5) obtained with 10^6 different initial functions φ belonging to $\mathscr{I}$.

The most noticeable feature of Fig. 10 is the presence of regions that are either completely black or completely white. These regions were numerically investigated to test for the presence of black dots in completely white regions and vice versa. The numerical results are consistent with the existence of sets of positive measure in (t_1,t_2) space which are associated with only one type of limit cycle. This feature is accentuated in Figs. 11 and 12, which are similar to Fig. 10, but with the parameters of Fig. 8. The relative abundance of short limit cycles in the space of control parameters illustrated in Fig. 9 is related to the existence of these sets which appear to have positive Lebesgue measure on the (t_1,t_2) square. Based on extensive digital simulations, it appears that there is no upper bound on the order of the multistability displayed by Eq. (5), and the more finely one looks at the structure in (t_1,t_2) space, the more new limit cycles (of different period) one is likely to find (see Fig. 12). This behavior was not observed in the systems with a continuous nonlinearity discussed in Secs. II A and II B.

The existence of positive area subsets of the basins is important since it suggests the existence of regions in the space of initial functions which are stable in the sense that for IFs in these subspaces, the asymptotic solution evolu-

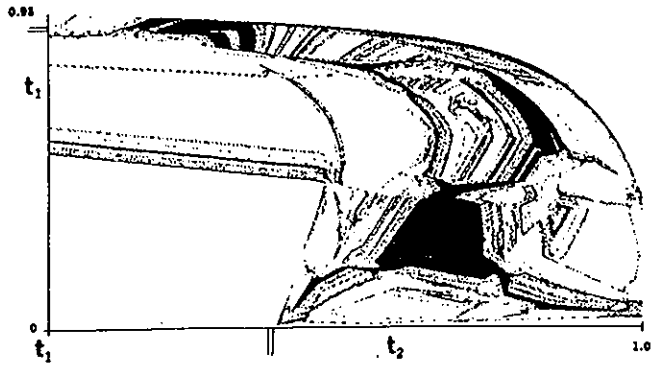

FIG. 11. Subsets of the basins of attraction of the three solutions of (5) displayed in Figs. 8(a)–8(c). The black dots represent values of (t_1,t_2) such that $\varphi \in \mathscr{I}$ generates the solution of Fig. 8(b). The two small bars on each axis mark a region which is enlarged in the next figure.

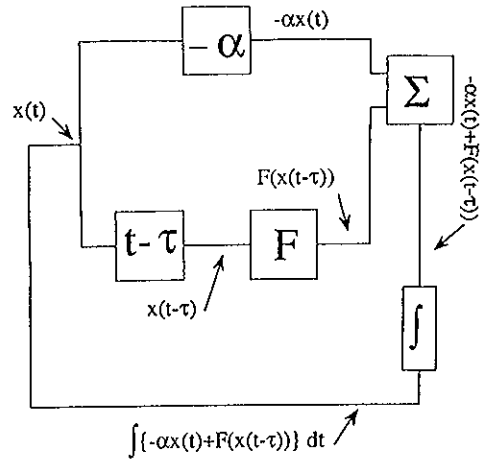

FIG. 13. Schematic diagram of the electronic analog computer.

tion is independent of small variations of the initial system preparation. This property is found in the continuous examples of Sec. II, and is therefore not a consequence of the discontinuous nonlinearity in (5).

We have, to this point, been concerned by the dynamics of purely deterministic DDEs. Although these equations play an important role in the modeling of real physical situations, it is obvious that any experimentalist must deal with a given amount of noise. There are numerous discussions in the literature of situations where minute stochastic perturbations can have a dramatic effect on the underlying dynamics. It is therefore interesting to know whether the multistability discussed here is also observed in a real physical system designed to be accurately modeled by a first order nonlinear DDE. This question is examined in the next section with the help of a task specific electronic analog computer.

IV. AN ANALOG STUDY OF MULTISTABILITY

In this section, we investigate the dynamics of Eq. (5) with an electronic analog computer. The main motivation behind this work is to assess the potential of analog computation for the analysis of DDEs. In addition to allowing rapid explorations of parameter space, analog computations are useful to investigate global stability and quantify the influence of noise on the solutions. Another motivation stems from recent experimental studies of (delayed) neural control loops, involving, e.g., the pupil light reflex[33] and delayed visual tracking tasks.[13] The analog computer provides a testbench for these experimental protocols which also make use of analog delay lines (described in the Appendix).

The techniques of analog computation for noisy nonlinear systems are described in Ref. 34. The analog computer designed to study Eq. (5) is a closed electronic circuit. The details of the design can be found in Ref. 29. Since analog differentiation leads to instability, Eq. (5) is simulated in its integral form

$$x(t)=\int_{t_0}^{t}[-\alpha x(s)+F(x_\tau(s))]ds+x(t_0),$$

where

$$\begin{cases} t \geqslant t_0, \\ s \geqslant -\tau. \end{cases} \tag{7}$$

The circuit, shown schematically in Fig. 13, multiples the signal $x(t)$ by a factor α, delays it by τ, and transforms it according to the static nonlinearity F, sums the resulting signals and integrates the sum. The result of the integration is equated with the original signal $x(t)$ at the point where the loop is closed and the voltage $x(t)$ monitored. The initial state φ of the circuit consists in the turn-on state of the component—described in the Appendix—which provides the delay in the analog computer. Some details of the analog computer design are given in the Appendix. Precise wiring diagrams, calibration procedures, and error calculation methods are available from the authors. These lengthy details cannot be included here.

Figure 14 shows four analog solutions. The periodic solutions are compared with the analytical solutions of (5) obtained at the same parameter values for constant initial functions (when the solution is aperiodic, it is impossible to measure the parameters in the circuit with enough pre-

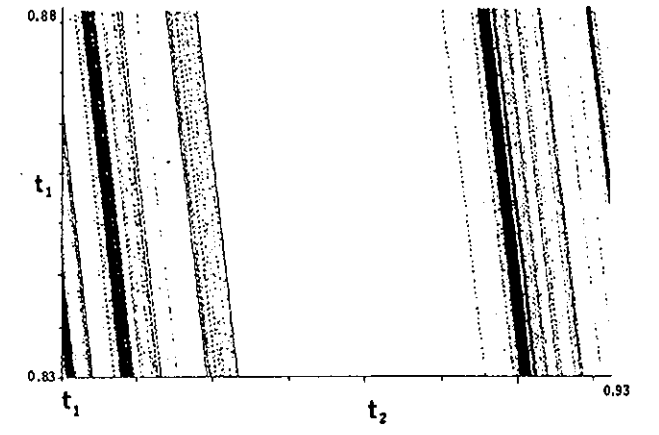

FIG. 12. Enlarged view of the small region of Fig. 11 marked on the axes.

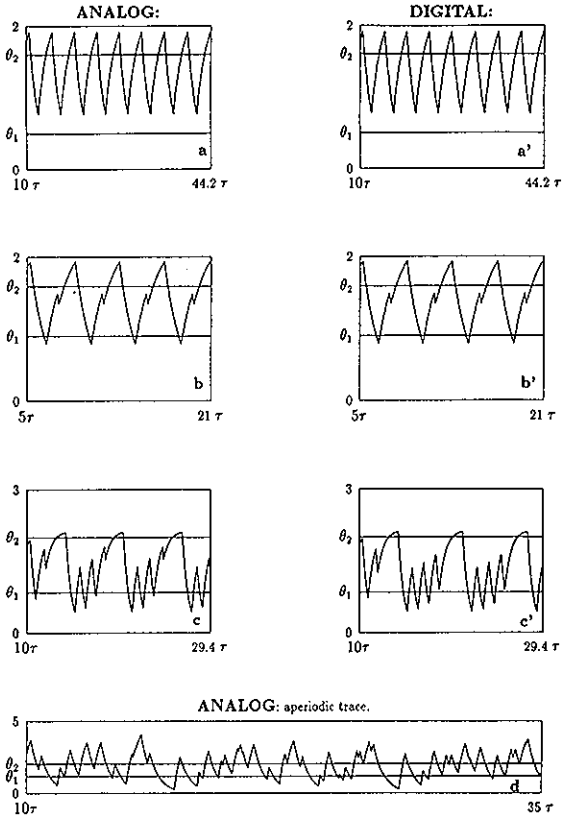

FIG. 14. Analog and digital simulations of Eq. (5). The initial functions were constant and $\varphi(t) \in [\theta_1, \theta_2]$ in all cases. In panels (a) and (a'), the parameters of (5) were $\theta_1 = 0.5$; $\theta_2 = 1.6$; $\alpha = 0.6$; $c = 2.4$; $\tau = 1$. In (b) and (b'), $\theta_1 = 0.9$; $\theta_2 = 1.6$; $\alpha = 0.8$; $c = 3.2$; $\tau = 1$. In (c) and (c'), $\theta_1 = 0.86$; $\theta_2 = 2$; $\alpha = 1.5$; $c = 3.2$; $\tau = 1$. In (d), it is not possible to measure with meaningful accuracy all the necessary parameters on the analog computer when the trace is highly irregular, thus we do not give a digital trace to compare with the analog solution. However, solutions similar to (d) can be obtained numerically in the following region of parameter space: $\theta_1 \simeq 0.8$; $\theta_2 \simeq 2$; $\alpha \simeq 1.5$; $c \simeq 3.2$; $\tau \simeq 1$.

cision to compare aperiodic digital and analog solutions). For simple limit cycles, the agreement between the two is excellent: Discrepancies between the amplitude and period of the two are on the order of 0.5%. This agreement decreases as the solution complexity (i.e., the number of extrema per period) increases. In fact, systematic shifts in parameter space seem to occur; small shifts lead to quantitative disagreement, while larger shifts cause qualitative differences, e.g., in the number of maxima per period. Nevertheless, it appears that the analog solutions correspond to analytic solutions of (5). Discrepancies between analytical and analog solutions are due to noise and to errors in the estimation of parameters.

Although the signal to noise ratio in our circuit was large (about 100:1), the exact influence of the noise on these dynamics is not well understood. Nonlinear dynamical systems can be sensitive to even minute stochastic perturbations, especially when the dynamics are chaotic or the system is operating in the vicinity of bifurcation points or when trajectories come close to basin boundaries.[24] Although the topic of stochastic DDEs remains virtually undeveloped, there have been investigations of noise-induced transitions in equations such as (1)[35,36] and (5).[37] For this latter case, colored noise has been shown to perturb the period more than the amplitude of solutions, especially near bifurcation points. In our study, fluctuations in both amplitude and period are expected.[37]

The important point is that the solutions of (5) are observable despite the electronic noise, and thus that the solutions are stable in the function space in which they evolve. One way to visualize this is as follows. In the same way every point on a trajectory of an ordinary differential equation belongs to the basin of attraction of the solution toward which it tends asymptotically, every function defined on an interval $(t, t+\tau)$ of a solution belongs to the basin of attraction of the DDE in function space. Our experiments show that this set of functions, along with their perturbations (which are much larger than for the analytical solutions which are accurate to one part in 10^{12}), thus also belong to the basin of attraction of the asymptotic solution.

A. Bifurcations to complex limit cycles

We now discuss the behavior of the circuit as α, θ_1, and θ_2 are varied, and compare the analog solutions with the analytic solutions of Eq. (5), the latter obtained by plotting (6) with a digital computer. Unless otherwise specified, the initial function φ is a constant, and c is fixed. When θ_1 and θ_2 are sufficiently far apart, the solution oscillating around θ_2 does not cross the positive feedback threshold and the feedback in (5) is purely negative. In this case, both the electronic and analytic solutions have similar shape and offset, though the values of the amplitudes may differ by $\sim 0.5\%$ (see Fig. 14, panels a and a').

As $\theta_1 \to \theta_2$, the same approximate sequence of bifurcations is observed in both the analog and digital solutions. However, some complex analytic limit cycles were not observed on the analog computer; in fact, digital simulations indicate that the regions of parameter space in which these cycles are stable are often smaller than the errors on the measured parameters. Nevertheless, the gradual increase in complexity (i.e., the number of extrema per period) of x as $\theta_1 \to \theta_2$ is observed in the circuit. In particular, when the two thresholds are sufficiently close, the analog solutions appear to be aperiodic [an example of such a solution is displayed in Fig. 14(d)].

One very interesting feature displayed by the electronic solution is the appearance of spiral-type limit cycles in the vicinity of an unstable homoclinic cycle, as shown in Fig. 14(c). This phenomenon is described in Ref. 26, where the DDE is reduced to a one-dimensional map of the unit interval onto itself. This type of solution is borne out of an unstable periodic solution around the lower threshold, the instability being due to positive feedback. As α is increased, the length of the residence time of the solution around θ_1 increases. Again, there are discrepancies between the values of α generating the same electronic and analytic solutions.

B. Multistability and hysteresis

The initial state of the analog delay line (BBD, see the Appendix) used to provide the delay in the electronic loop corresponds to the initial function φ for the DDE. All the properties of the analog oscillator discussed to this point have been obtained with constant initial voltages in the BBD corresponding to a constant initial function φ. The parameters in the analog computer were set and then the loop was closed. In the part of the experiment described in the previous section, parameters were not changed after oscillation onset to allow for a comparison between experimental observations and analytic solutions. Alternately, the parameters can be changed continuously as the analog computer is oscillating. When parameters θ_1 and/or α are varied in this fashion without reinitializing the system, a range of nonconstant initial functions is explored as the system evolves since the solution on any interval $(t,t+\tau)$ is the initial function for the ensuing solution.

As the threshold θ_1 is slowly increased toward θ_2 (and the circuit is allowed to stabilize), solutions undergo a series of bifurcations toward ones of higher period; cf. Fig. 14. When θ_1 approaches the second threshold (θ_1 above 2 V for $\theta_2=3.2$ V), the solution decays to the lower asymptote (about 1 mV above ground). As θ_1 is subsequently decreased, the first oscillatory solution observed in the system is the slowest limit cycle corresponding to a pure negative feedback situation. Thus different solutions of Eq. (5) are found at the same parameter values depending on whether θ_1 is being increased or decreased. The only difference in behavior between the rise and the fall of θ_1 is the initial condition for the system. This *hysteresis* in the bifurcation structure indicates the presence of multistability in the system.

To examine the sensitivity of solution behavior on the initial function, the analog computer was modified to allow for an arbitrary initial function to be entered into the BBD. An electronic switching circuit opens the feedback loop to permit the loading of an initial function. Our design allows for the accurate control of the voltages on each of the capacitors of the BBD by interfacing it with a digital computer, in which the desired initial function is stored. The rest of the circuit is always initialized to the same state, i.e., with one extremity of the loop grounded, while the other one receives a programmed initial function from the digital computer through a D/A board. The BBD receives the signal containing the initial function as well as a sampling pulse from the digital computer. The electronic switch is used to close the loop once the initial function is sent and the analog computer is once again autonomous.

Solution dependence on the initial function was investigated for the class of functions $\varphi\in\mathscr{I}$ introduced in Sec. III (see Fig. 6). Recall that the evolution of $x(t)$ for $t>0$ depends only on $\{t_1,t_2\}$ [for fixed $x(0)$] because the forcing term F is piecewise constant.

Figure 15 reveals that at least two periodic solutions co-exist, each with its own basin of initial functions from this class. As t_2 is varied between t_1 and 0, the interval $[t_1,0]$ splits into two sets of t_2 values, one yielding a short period solution and the other, a long period solution. This

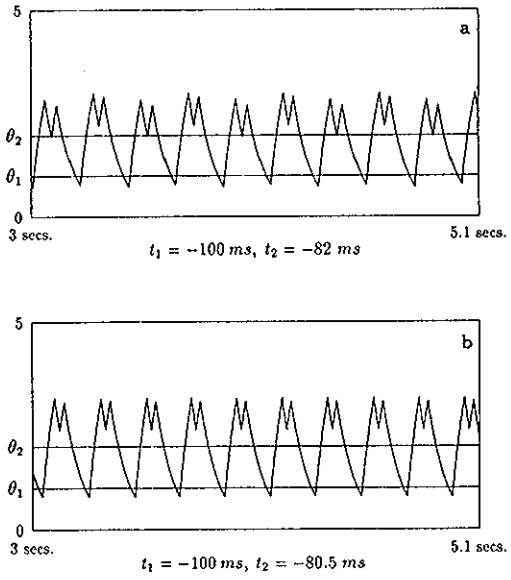

FIG. 15. Bistable solutions of Eq. (5) obtained with the electronic analog computer. The parameters in both panels are $\theta_1=1$, $\theta_2=2$, $\alpha=3.57$, $c=18.7$, $\tau=143$ ms. Transients were discarded. In panel (a), the parameters for the initial function are $t_1=-100$ ms; $t_2=-82$ ms. In panel (b), $t_1=-100$ ms; $t_2=-80.5$ ms.

separation of the interval $[t_1,0]$ into sets yielding different limit cycles confirms the existence of multistability. This type of analog solution multistability was observed for large ranges of parameters when the initial function $\varphi\in\mathscr{I}$, although the structure of the sets is complicated and cannot be determined with the analog computer. Nevertheless, the multistability observed digitally is also observed in an inevitably noisy electronic analog computer, whose temporal evolution can depend in a very sensitive way on the experimental preparation.

V. CONCLUSION

We have discussed the presence of multistability in three first-order nonlinear differential delay equations. Although bistability has been previously noted in such systems,[9,20,25,22,21] we report here on the sensitivity of the solution behavior on perturbations of the initial function. For the logistic DDE (Sec. II A), the basins of attraction of bistable limit cycles possess a complicated structure at all numerical scales. This is also the case for the basins of attraction of bistable and tristable limit cycles in an integrable nonlinear DDE with a piecewise constant nonlinearity (Sec. III).

The nature of the bistability present in the Mackey–Glass equation (Sec. II A) is somewhat simpler than that found in the two other systems mentioned above. More precisely, a symmetry in this equation [i.e., its invariance under the transformation $x(t)\to -x(t)$] is responsible for the bistability between positive and negative limit cycles. In addition, the structure of the boundaries separating the basins of attraction of these solutions seems to be quite regular. This makes the Mackey–Glass equation (or any DDE displaying the same symmetry) a plausible candidate

for further analytic work. Our study of the Mackey–Glass system leads us to the conclusion that at least one possible mechanism for bistability in a DDE is its invariance under a coordinate transformation.

Finally, in an electronic analog computer designed to integrate a nonlinear DDE, we observe the sensitive dependence of the evolution of the system to perturbations of the initial function (Sec. IV). This shows that such sensitivity is present in real physical systems with delays and noise, and therefore that it should be considered when studying the dynamics of such systems experimentally.

ACKNOWLEDGMENTS

We wish to thank the Natural Sciences and Engineering Council of Canada (NSERC) for operational and equipment grants for this research and NATO for a collaborative research grant for M.C.M. High precision numerical algorithms for nonlinear DDEs were graciously provided to us by Abderrazek Karoui, University of Ottawa, to check the precision of our own. We thank him for his kindness and cooperation.

APPENDIX: OVERVIEW OF THE ANALOG COMPUTER

In this Appendix we give a brief description of the design of the analog computer used to integrate Eq. (5). The details concerning the circuit, calibration procedure, and error calculations (too lengthy to be included here) can be found in Ref. 29 or requested from the authors.

This analog computer is in a sense an analog-digital hybrid because the delay is synthesized by a digital integrated circuit called an analog delay line, or bucket brigade device (BBD, RD 5108 from EG&G Reticon). This CMOS device samples and delays the signal by storing it in an array of 1024 capacitor circuits. Each of these capacitors (buckets) transfers its charge to the neighboring capacitor at every other logic HIGH of the sampling signal or clock (typically a square wave). The delay is proportional to the number of buckets and inversely proportional to the experimentally controlled clock frequency. The delay was kept at $\tau = 300 \pm 1$ ms for the results presented here (except when specified explicitly). The output of the delay circuit was fed through an eight-pole Bessel filter to remove the sampling artifact. The feedback function F in Eq. (5) is simulated electronically with an LM 393 monolithic comparator circuit. The thresholds θ_1 and θ_2 are voltages controlled by potentiometers. The output of this stage is 5 V when the input is in the interval $[\theta_1, \theta_2]$ and at ground otherwise, thus simulating the piecewise constant nonlinearity in Eq. (5). The rest of the circuit uses standard op-amp technology, although the design of the integration stage requires particular care. For the delays used in this study, the dominant frequency of the solutions is in the 1 Hz range, thus requiring a good low-frequency integrator with low drift.

To evaluate circuit performance, it is necessary to compare the electronic solutions with the analytic solutions (6), plotted using a digital computer. The parameters used for the latter are measured on the electronic circuit (e.g., the gain α, the delay τ produced by the BBD, etc.). Their measurement is not straightforward, since each stage introduces extra gains and offsets which make it deviate from its ideal desired behavior. For example, the BBD operates with maximal linearity when the input is slightly biased. Also, the gain of the integrator is closely linked to its cutoff frequency, and the frequency of the signal to be integrated is the main factor influencing the choice of values for the resistors and capacitors making up the integration stage, regardless of its total gain. Consequently, the integrator introduces a gain which adds to that of the stage simulating the amplification α [see (5)]. An equation has been derived to connect the circuit parameters to those used in the analytic solutions.[29]

The first electronic solutions to be compared with analytic solutions are the steady states corresponding to the asymptotes 0 and γ in (6). The upper asymptote can be measured with an accuracy of about 0.1%, and we can relate this value to the ratio c/α using the circuit equation mentioned above (typically this value varies between 5 and 20, for periodic and chaotic behavior). The lower asymptote fluctuates around zero with an amplitude of $\simeq 1$ mV. Both asymptotes are stable over periods well beyond 12 h, and the simpler periodic solutions were also stable over this time span. The more complicated solutions (e.g., those crossing either θ_1 and/or θ_2 more than five times in one delay) were stable for shorter periods ranging from seconds to hours depending on the number of extrema per period, their proximity to the thresholds θ_1 and θ_2, and the noise level in the circuit.

[1] G. Julia, J. Math. Pures Appl. **4**, 47 (1918).
[2] P. Fatou, Bull. Soc. Math. France **47**, 271 (1919)
[3] C. Grebogi, E. Ott, and J. A. Yorke, "Chaos, strange attractors, and fractal basin boundaries in nonlinear dynamics," Science **238**, 632 (1987).
[4] C. Grebogi, E. Ott, J. A. Yorke, and H. E. Nusse, "Fractal basin boundaries with unique dimension," Ann. N.Y. Acad. Sci. **497**, 117 (1987).
[5] S. McDonald, C. Grebogi, E. Ott, and J. A. Yorke, "Structures and crises of fractal basin boundaries," Phys. Lett. A **107**, 51 (1985).
[6] B. Dorizzi, B. Grammaticos, M. Leberre, Y. Pomeau, E. Ressayre, and E. Tallet, "Statistics and dimension of chaos in differential delay systems," Phys. Rev. **35** A (1), 328 (1987).
[7] J. D. Farmer, "Chaotic attractors of an infinite dimensional dynamical system," Physica D **4**, 366 (1982).
[8] F. A. Hopf, P. Meystre, P. D. Drummond, and D. F. Walls, "Anomalous switching in dispersive optical bistability," Opt. Comm. **31**, 245 (1982).
[9] K. Ikeda and K. Matsumoto, "High dimensional chaotic behavior in systems with time delayed feedback," Physica D **29**, 223 (1987).
[10] K. Ikeda and O. Akimoto, "Successive bifurcations and dynamical multistability in a bistable optical system: A detailed study of the transition to chaos," Appl. Phys. B **28**, **170** (1979).
[11] K. Ikeda, "Multiple-valued stationary state and instability of the transmitted light by a ring cavity system," Opt. Commun. **30**, 257 (1979).
[12] H.-J. Zhang, J.-H. Dai, P.-Y. Wang, F.-L. Zhang, G. Xu, and S.-P. Yang, "Chaos in liquid crystal optical bistability," *Directions in Chaos*, edited by B.-L. Hao (World Scientific, Singapore, 1988), p. 46.
[13] A. Beuter, J. G. Milton, C. Labrie, L. Glass, and S. Gauthier, "Delayed visual feedback and movement control in Parkinson's disease," Exp. Neurol. **110**, 228 (1990).
[14] A. Beuter, J. G. Milton, C. Labrie, L. Glass, and S. Gauthier, "Delayed visual feedback and movement control in Parkinson's disease," Exp. Neurobiol. **110**, 228 (1990).
[15] M. C. Mackey and J. G. Milton, "Feedback, delays and the origin of

blood cell dynamics," Commun. Theor. Biol. **1** (5), 299 (1990).
[16] C. M. Marcus and R. M. Westervelt, "Stability of analog neural networks with delay," Phys. Rev. A **39**, 347 (1989).
[17] M. C. Mackey, "Commodity price fluctuations: Price dependent delays and nonlinearities as explanatory factors," J. Econ. Theory **48** (2), 497 (1989).
[18] U. an der Heiden, in *Delay Equations, Approximation and Application*, edited by G. Meinardus and G. Nurnberger (Birkhauser, Basel, 1985); Intern. Ser. Num. Math. **74**.
[19] A. F. Ivanov and A. N. Sharkovskiĭ, "Oscillations in singularly perturbed delay equations," in *Dynamics Reported*, edited by H. O. Walter and U. Kirchgraber (Springer-Verlag, New York, 1991); **3**, 165 (1991).
[20] D. L. Kaplan, H. M. Gibbs, F. A. Hopf, and R. L. Shoemaker, "Observation of chaos in optical bistability," Phys. Rev. Lett. **46**, 474 (1981).
[21] R. Vallée and C. Delisle, "Periodicity windows in a dynamical system with delayed feedback," Phys. Rev. A **34**, 309 (1986).
[22] R. Vallée and C. Delisle, "Mode description of the dynamical evolution of an acousto-optic bistable device," IEEE J. Quantum Electron. **QE-21**, 1423 (1985).
[23] K. Ikeda, K. Kondo, and O. Akimoto, "Successive higher harmonic bifurcations in systems with delayed feedback," Phys. Rev. Lett. **49**, 1467 (1982).
[24] J. M. Aguirregabiria and J. R. Etxebarria, "Fractal basin boundaries of a delay differential equation," Phys. Lett. A **122**, 241 (1987).
[25] J.-N Li and B.-L Hao, "Bifurcation spectrum of a delay differential system related to optical bistability," Commun. Theor. Phys. **11**, 265 (1989).
[26] U. an der Heiden and M. C. Mackey, "The dynamics of production and destruction: Analytic insight into complex behavior," J. Math. Biol. **16**, 75 (1982).
[27] M. C. Mackey and L. Glass, "Oscillation and chaos in physiological control systems," Science **197**, 287 (1977).
[28] A. Longtin, "Nonlinear oscillations, noise and chaos in neural delayed feedback, Ph.D thesis, McGill University (1989).
[29] J. Losson, "Multistability and probabilistic properties of delay differential equations," Master's thesis, McGill University (1991).
[30] M. C. Mackey, *Time's Arrow: The Origin of Thermodynamic Behavior* (Springer-Verlag, Berlin, 1992).
[31] D. Babai, "Sur une équation différentielle à délai modélisant des processus de contrôles physiologiques," Master's thesis, Université de Montréal (1990) (in French).
[32] H.-O Walther, "Homoclinic solution and chaos in $\dot{x}(t)=f(x(t-1))$," Nonlin. Anal. **5**, 775 (1981).
[33] J. G. Milton and A. Longtin, "Evaluation of pupil constriction and dilation from cycling measurements," Vision Res. **30**, 515 (1990).
[34] F. Moss and P. V. E McClintock (Editors), *Noise in Nonlinear Dynamical Systems* (Cambridge University, Cambridge, 1989), Vol. 3, Chap. II.
[35] R. Kapral, E. Celarier, P. Mandel, and P. Nardone, "Noisy delay differential equations in optical bistability," SPIE Optical Chaos **667**, 175 (1986).
[36] A. Longtin, "Noise induced transitions at a Hopf bifurcation in a first order delay-differential equation," Phys. Rev. A **44**, 4801 (1991).
[37] A. Longtin, J. G. Milton, J. Bos, and M. C. Mackey, "Critical behavior of the pupil light reflex at oscillation onset," Phys. Rev. A **41**, 6992 (1990).